# On second harmonic generation and multiphoton-absorption induced luminescence from laser-reshaped silver nanoparticles embedded in glass

Zolotovskaya, Svetlana; Tyrk, M. A.; Stalmashonak, A.; Gillespie, W. A.; Abdolvand, A.

*Published in:*
Nanotechnology

*DOI:*
10.1088/0957-4484/27/43/435703

*Publication date:*
2016

# On second harmonic generation and multiphoton-absorption induced luminescence from laser-reshaped silver nanoparticles embedded in glass



2016 Nanotechnology 27 435703

(http://iopscience.iop.org/0957-4484/27/43/435703)

OPEN ACCESS
IOP Publishing
Nanotechnology

Nanotechnology **27** (2016) 435703 (8pp)
doi:10.1088/0957-4484/27/43/435703

# On second harmonic generation and multiphoton-absorption induced luminescence from laser-reshaped silver nanoparticles embedded in glass

**S A Zolotovskaya[1,4], M A Tyrk[2,4], A Stalmashonak[3], W A Gillespie[2] and A Abdolvand[2]**

[1] Materials Science Institute, Engineering Department, Lancaster University, Lancaster LA1 4YW, UK
[2] Materials & Photonic Systems Group, School of Science & Engineering, University of Dundee, Dundee DD1 4HN, UK
[3] CODIXX AG, Steifeldstr. 3, D-39179 Barleben, Germany

E-mail: a.abdolvand@dundee.ac.uk

Received 15 July 2016, revised 17 August 2016
Accepted for publication 31 August 2016
Published 23 September 2016

**Abstract**

Spherical silver nanoparticles (NPs) of 30 nm diameter embedded in soda-lime glass were uniformly reshaped (elongated) after irradiation by a linearly polarised 250 fs pulsed laser operating within the NPs' surface plasmon resonance band. We observed second harmonic generation (SHG) and multiphoton-absorption-induced luminescence (MAIL) in the embedded *laser-reshaped* NPs upon picosecond (10 ps) pulsed laser excitation at 1064 nm. A complementary study of SHG and MAIL was conducted in soda-lime glass containing embedded, *mechanically-reshaped* silver NPs of a similar elongation ratio (aspect ratio) to the *laser-reshaped* NPs. This supports the notion that the observed difference in SHG and MAIL in the studied nanocomposite systems is due to the shape modification mechanism. The discrete dipole approximation method was used to assess the absorption and scattering cross-sections of the reshaped NPs with different elongation ratios.

Keywords: surface plasmon resonance, metal-glass nanocomposites, metallic nanoparticles, nonlinear properties

(Some figures may appear in colour only in the online journal)

## 1. Introduction

Metallic nanoparticles (NPs) have gained a great deal of attention in recent years due to their unique linear and nonlinear optical properties. These properties result from localised surface plasmon resonances (SPRs) originated from collective charge density oscillations of free electrons in metal particles. Alkali-rich glass of soda-lime variety has been proposed as one of host matrices for the formation of embedded silver (Ag) NPs [1], thus forming a Metal-Glass Nanocomposite (MGN). It was shown that optical and structural properties of the MGNs are easily manipulated upon irradiation with nano-, pico- and femtosecond pulse laser sources [2–8]. Ultra-short-pulse laser irradiation is a well-established *spatially selective* method for Ag NP shape modification, which depends strongly on the polarisation state of the incident laser beam. For instance, linearly polarised irradiation at low intensity ($\leqslant 0.5\,\mathrm{TW\,cm^{-2}}$) leads to the formation of Ag nano-ellipsoids with their long axis aligned

[4] Authors contributed equally to this work.



 

along the laser polarisation direction [3, 5, 6]; circular polarisation leads to the formation of nano-discs; radial (or azimuthal) polarisation results in a set of ellipsoids orientated in the directions reflecting the local polarisation state of the incident beam [9]. Laser-assisted shape modification of NPs leads to the observation of *local* optical dichroism achieved via spatially selective modification of the SPR position depending on the laser parameters. On the other hand, simultaneous heating and tensile deformation of MGNs results in *global* shape modification of Ag NPs, producing uniformly orientated ellipsoids in the volume of the glass matrix. These mechanically stretched MGNs are routinely used as high-contrast polarisers [10], and have also demonstrated second harmonic generation (SHG) when subjected to femtosecond pulse laser excitation at 800 nm [11].

In this paper, for the first time to our knowledge, we demonstrate SHG from *locally* reshaped (*laser-reshaped*) Ag NPs embedded in soda-lime glass. The spectrally resolved nonlinear optical response in these MGNs revealed the presence of multiphoton-absorption-induced luminescence (MAIL) along with the SH signal. Complementary studies of SHG were carried out in a mechanically stretched MGN containing ellipsoidal Ag NPs with a similar aspect ratio. The dependence of SHG and MAIL on the aspect ratio of Ag nano-ellipsoids in the laser-reshaped MGNs is reported and compared to the results of modelling obtained using a discrete dipole approximation (DDA) approach [12].

## 2. Experimental techniques

*Two* glass substrates ($40 \times 40\ \mathrm{mm}^2$) containing spherical Ag NPs (*MGN-I* and *MGN-II*) were used for SHG measurements (figure 1). In both cases, the formation of Ag clusters in the glass matrix was achieved via a thermally assisted $Ag^+/Na^+$ ion-exchange process—described in detail elsewhere [13–15]. A 1 mm soda-lime silica float glass (glass composition in wt.-%: 72.5 $SiO_2$, 14.4 $Na_2O$, 6.1 CaO, 0.7 $K_2O$, 4.0 MgO, 1.5 $Al_2O_3$, 0.1 $Fe_2O_3$, 0.1 MnO, 0.4 $SO_3$) was immersed in a mixed melt of $AgNO_3$ and $KNO_3$ at 400 °C (for a duration of 30 min at 400 °C in a mixed melt of 2 weight-% $AgNO_3$ and 98 weight-% $KNO_3$) and was subsequently annealed at about 500 °C in a $H_2$ reduction atmosphere for approximately 12 h [15]. This resulted in the formation of *spherical* Ag particles of $30 - 40$ nm in diameter in ~20 $\mu$m surface layers on both sides of the glass sample. Single-sided samples were produced by removal of the nanoparticle-containing layer from one side of the samples by etching the samples in a solution of 12% hydrofluoric acid. An extinction spectrum of the samples containing spherical Ag NPs (shown in figure 1(a)—black line) exhibits a strong SPR band at ~430 nm, which is consistent with the NP size.

### 2.1. Introducing MGN-I

The laser-assisted reshaping of one of the MGNs (henceforth called *MGN-I*) was conducted using a 250 fs Yb:KGW laser system (PHAROS laser, Light Conversion Ltd) equipped with a collinear optical parametric amplifier (ORPHEUS OPA, Light Conversion Ltd) operating at 500 kHz. The laser beam was focused into a spot of 30 $\mu$m full width at $1/e^2$ intensity level. Figure 1(c) shows *four* areas of $5 \times 5\ \mathrm{mm}^2$ of *MNG-I* sample that were irradiated with different laser parameters in order to achieve different Ag ellipsoid aspect ratios (the $R = a/b$ ratio of the long $a$ to short $b$ axis). After the first irradiation step (Irradiation 1, table 1) for FEM A−D, the laser was tuned to an off-resonance position (Irradiation 2, table 1) for one of the irradiated areas, namely FEM D. This subsequent irradiation at 750 nm (long-wavelength side of the already modified SPR) allowed for further elongation of the NPs and led to the aspect ratio of $R \sim 4.1$ in FEM D, hence pronounced optical dichroism in comparison to what is expected after only a single-wavelength irradiation [5]. The employed laser parameters are summarised in the table 1.

The polarised extinction spectra of *MGN-I* sample were measured using a spectrophotometer (JASCO V-670 UV/VIS/NIR) and are shown in figure 1(a). After laser irradiation the original SPR band of the spherical Ag NPs, peaked at about 430 nm, splits into *two* polarisation dependent bands (FEM A, B, C, and D) with the long axis of the NPs being orientated along the laser polarisation (p-polarisation). The p-polarised SPR bands for all four irradiated areas are shown in figure 1(a). It can be seen that consecutive irradiations at longer wavelengths lead to a larger spectral gap between the polarised SPR bands (larger red-shift of the p-polarisation) thus confirming increase in the aspect ratio of the reshaped NPs with the maximum laser-assisted elongation achieved for FEM D sample. The observed residual absorption at 430 nm in all laser-reshaped samples are due to the presence of some unmodified spherical Ag NPs within the NP containing layer and further away from the *MGN-I* sample surface. Furthermore, in FEM D sample the residual peak at ~580 nm is also due to the 'non-modified' NPs after the second irradiation (subsequent irradiation). Therefore, FEM D contains reshaped NPs with aspect ratios of both 2.6 and 4.1.

### 2.2. Introducing MGN-II

The mechanical reshaping of Ag NPs was carried out by subjecting a 1 mm thick MGN sample with a nanoparticle-containing layer of about 20 $\mu$m to tensile deformation with simultaneous heating below the transition temperature of the glass [21]. This results in uniformly orientated Ag ellipsoids without visible stress-induced birefringence in the glass matrix, figure 1(d). After mechanical deformation the total thickness of the *MGN-II* sample and nanoparticle-containing layer were reduced to ~200 $\mu$m and 4 $\mu$m, respectively. The polarised extinction spectra of the mechanically stretched *MGN-II* are shown in figure 1(b), showing splitting of the SPR band. The increased bandwidth of the p-polarised SPR band is due to uniform deformation of Ag NPs. The aspect ratio of the mechanically stretched Ag NPs was estimated to be ~4.9.

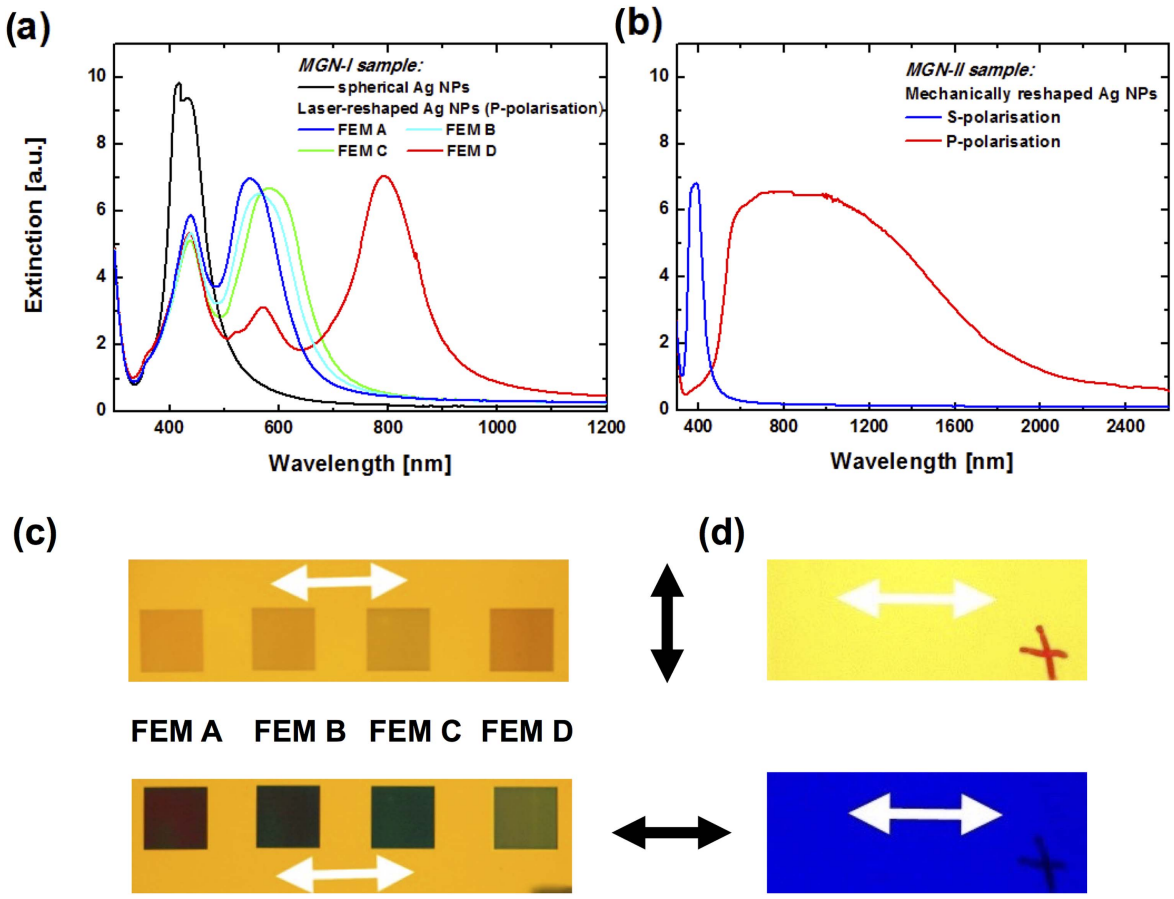


**Figure 1.** Note that p-polarisation is for the light polarised parallel to the long axis while s-polarisation is parallel to the short axis of the Ag prolate spheroids. (a) Polarised extinction spectra of the original MGN containing spherical Ag NPs (black line) and laser-reshaped Ag NPs (*MGN-I*). Here only p-polarisation spectra of *MGN-I* are shown. (b) Polarised extinction spectra of the sample containing mechanically reshaped Ag NPs (*MGN-II*). Here both s- and p-polarisation spectra of *MGN-II* are shown for clarity. Images of the laser (c) and mechanically (d) reshaped MGNs are taken in polarised light. Black arrows indicate the polarisation direction of the incident light; white arrows show the orientation of the long axis of the Ag nano-ellipsoids.

**Table 1.** Laser-assisted reshaping of MGNs: femtosecond pulse laser irradiation parameters ($\lambda_L$—laser wavelength; $P_p$—peak pulse intensity; $N_p$—number of pulses per spot; $\lambda_{SPR}$—*longitudinal* SPR peak position; $R$—aspect ratio). The work on estimating aspect ratios is explained in the text.

| | Irradiation 1 | | | Irradiation 2 | | | | |
|---|---|---|---|---|---|---|---|---|
| Sample | $\lambda_{L1}$ (nm) | $P_{p1}$ (TW cm$^{-2}$) | $N_{p1}$ | $\lambda_{L2}$ (nm) | $P_{p2}$ (TW cm$^{-2}$) | $N_{p2}$ | $\lambda_{SPR}$ (nm) | $R$ |
| FEM A | 515 | 0.362 | 200 | | | | 547 | 2.3 |
| FEM B | 515 | 0.362 | 300 | | | | 567 | 2.5 |
| FEM C | 515 | 0.317 | 500 | | | | 585 | 2.6 |
| FEM D | 515 | 0.317 | 500 | 750 | 0.288 | 500 | 792 | 4.1 |

### *2.3. Estimating aspect ratios*

The aspect ratios of the laser-reshaped Ag NPs, summarised in table 1, and also Ag NPs in *MGN-II* were estimated using Gans's extension of Mie theory for non-spherical particles [16]. The extinction coefficient $\gamma$ of randomly orientated particles in the dipole approximation is given by [16, 17]:

$$\gamma = \frac{2\pi N V \epsilon_m^{3/2}}{3\lambda} \sum_j \frac{(1/P_j^2)\epsilon_2}{\left(\epsilon_1 + \frac{1-P_j}{P_j}\epsilon_m\right)^2 + \epsilon_2^2}, \quad (1)$$

where $N$ is the number of particles per unit volume, $V$ is the particle volume, $\epsilon_m$ is the dielectric constant of the host medium, $\lambda$ is the wavelength of the interacting light, and $\epsilon_1$ and $\epsilon_2$ are the real and imaginary part of the dielectric constant of the metal inclusions. For the *three* axes $a$, $b$, and $c$ of the ellipsoid with dimensions $a > b$ and $b = c$, the depolarisation factors $P_j$ are defined as:

$$P_a = \frac{1-r^2}{r^2}\left[\frac{1}{2r}\ln\left(\frac{1+r}{1-r}\right) - 1\right], \quad (2)$$

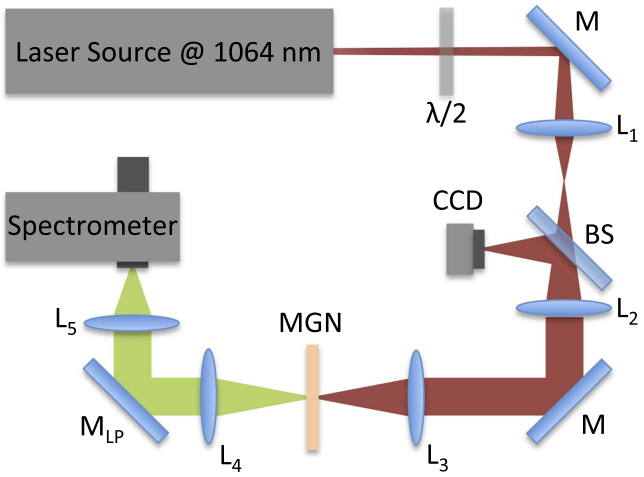


**Figure 2.** Schematic of the optical setup for SHG/MAIL measurements: $\lambda/2$–half-wave plate at 1064 nm; M–mirror; $L_1$ and $L_2$–a 1.3× laser beam expander; CCD–a CCD camera used for sample positioning, $L_3$–a 100 mm focal length lens; MGN–a metal-glass nanocomposite sample; $L_4$–a 75 mm focal length lens; $M_{LP}$–a longpass dichroic mirror with a cut-off wavelength at 900 nm; $L_5$–a 63 mm focal length lens.

$$P_b = P_c = \frac{1 - P_a}{2}, \tag{3}$$

where $r = \sqrt{1 - (b/a)^2}$.

This approach, was adopted in [18, 19] to simulate extinction spectra of gold nano-rods, demonstrated the *linear* relationship between the longitudinal SPR peak position and the aspect ratio of the nano-rods. Therefore it can be used to estimate the NPs elongation ratios for certain SPR band positions by considering that the resonance condition for the longitudinal mode is nearly fulfilled at [17]:

$$\epsilon_1 = -\frac{(1 - P_a)\epsilon_m}{P_a}. \tag{4}$$

For our estimates, the Ag dielectric constant was adopted from [20] and the host medium dielectric constant was 2.33 for the soda lime glass with the refractive index of 1.53. The real part of the dielectric constant for Ag was found to be almost linear in the spectral range from 500 to 900 nm: $\epsilon_1(\lambda) = 28.52 - 0.075\lambda_{SPR}$. Similarly $(1 - P_a)/P_a$ plotted as a function of the aspect ratio $R$ from 2 to 6 and linearised in accordance with: $(1 - P_a)/P_a = -4.64 + 4.35R$. The longitudinal SPR band positions were determined from the extinction spectra, figures 1(a), (b) and summarised in table 1.

### *2.4. SHG set-up*

Figure 2 illustrates the experimental arrangement. A linearly polarised 10 ps pulse laser at 1064 nm with a repetition rate of 200 kHz (Talisker Ultra, Coherent) was used as an excitation source for the SHG measurements. The measurements were performed in transmission geometry with the 1064 nm fundamental beam focused at normal incidence on the MGN sample surfaces. A half-wave plate ($\lambda/2$) at 1064 nm was employed to control the polarisation plane of the incident beam relative to the axes of the Ag nano-ellipsoids. A lens ($L_3$) with a focal length of 100 mm was used to focus the beam into ~64 $\mu$m diameter spot at $1/e^2$ intensity level. The SH signal was collected with a 75 mm focal length lens ($L_4$) and the fundamental beam was filtered out with a long-pass dichroic mirror ($M_{LP}$, 900 nm cut-off wavelength). The SH signal was then focused with a 63 mm focal length lens ($L_5$) on to the spectrometer (MS257, Oriel Instruments) equipped with a TE-cooled CCD at −70 °C (Newton 920, Andor). The MGNs were illuminated by the fundamental harmonic with fluences of up to 2 mJ cm$^{-2}$ to avoid photo-induced dissolution discussed elsewhere [22]. The accumulated signal (total *four* accumulations, each 1 s integration time) was analysed.

## 3. Results and discussion

In order to establish possible contributions to SH signal from the host matrix impurities, residual Ag ions and unmodified spherical Ag NPs, *three* sample groups of (*i*) undoped soda-lime glass, (*ii*) soda-lime glass doped with Ag ions, and (*iii*) soda-lime glass embedded with spherical Ag NPs (original MGN substrate before laser and/or mechanical modification) were investigated under identical experimental conditions. Neither SH nor MAIL signals were observed in any of the samples.

First, the dependence of SH intensity on the polarisation plane orientation of the laser operating at its fundamental harmonic of 1064 nm was investigated in the *MGN-II* sample containing mechanically reshaped Ag NPs. Since its SPR band position coincided well with the excitation wavelength, the highest incident field coupling and local field enhancement was expected. The polarisation plane of the laser beam was rotated relative to the long axis of elongated NPs by a $\lambda/2$-wave plate. The SH signal reached maximum for the fundamental harmonic polarised parallel to the long axis of the Ag NPs, i.e. for the fundamental harmonic polarisation angle equal to 0° (p-pol fundamental harmonic), as shown in figure 3(a).

The SH signal polarisation components, denoted as p-pol SH and s-pol SH in figure 3(b), were selected by placing a rotating polariser at the entrance slit of the spectrometer while keeping the polarisation plane of the fundamental beam parallel to the long axis of Ag NPs (p-pol fundamental harmonic). Two SH signal maxima were observed for p-pol SH where the SH polarisation plane is parallel to the long axis of the Ag nano-ellipsoids, at ±90° in figure 3(b). Therefore, the character of the SH signal obtained from *MGN II* is purely dipolar.

The spectrally resolved nonlinear optical response obtained in the laser reshaped (*MGN I*: FEM A, B, C & D) and mechanically reshaped (*MGN-II*) samples of MGN are shown in figure 4. The SH signal peaked at 532 nm accompanied by strong photo-induced luminescence can be seen in the spectra. The observed photoluminescence is attributed to the excitation via multiphoton absorption. Indeed, MAIL has been observed in a number of noble metal-based structures upon irradiation with ultra-short pulsed lasers [23–28]. For bulk metals the light emission follows the excitation of

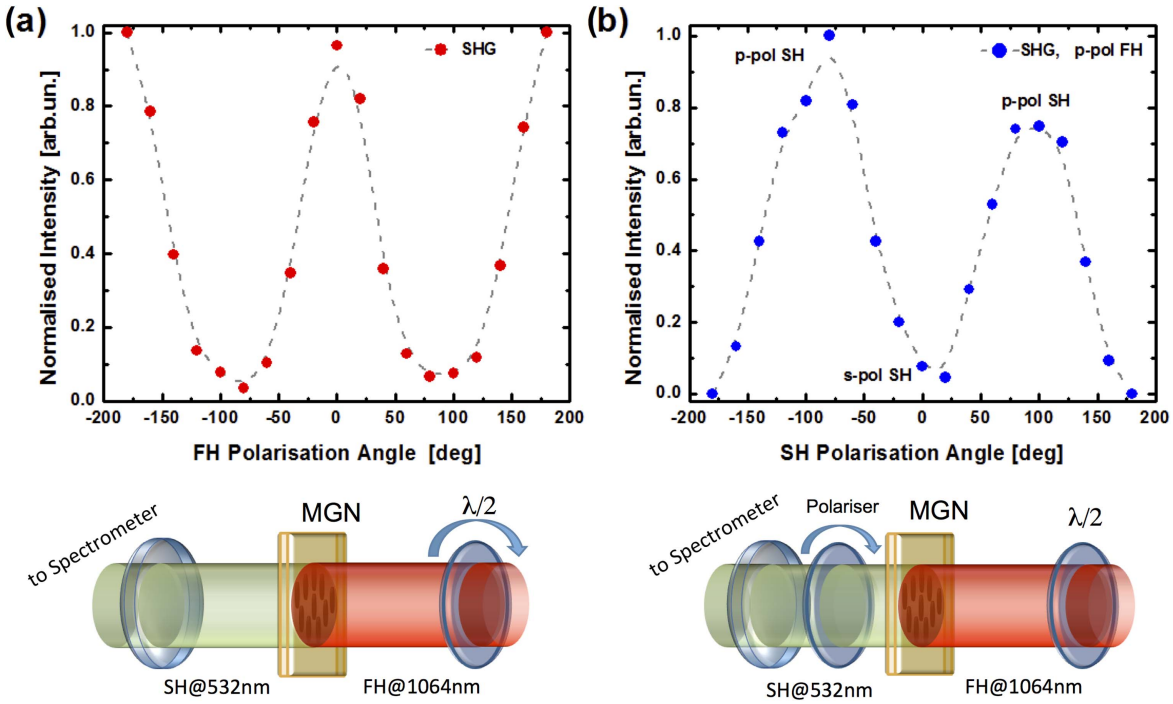


**Figure 3.** Measured SH intensity of mechanically reshaped MGN (*MGN-II*). (a) Polarisation dependence of SH signal intensity on orientation of the fundamental harmonic (*noted FH in the image for brevity*) beam polarisation plane (0 deg. corresponds to the incident excitation beam polarisation direction parallel to the long axis of Ag NPs). (b) SH signal polarisation components with the fundamental harmonic beam polarised parallel to the long axis of Ag NPs, p-pol fundamental harmonic (p-pol SH and s-pol SH are the SH signals polarised parallel to the long and short axes of Ag NPs respectively). Corresponding schematics of the experimental conditions are also shown for clarity.

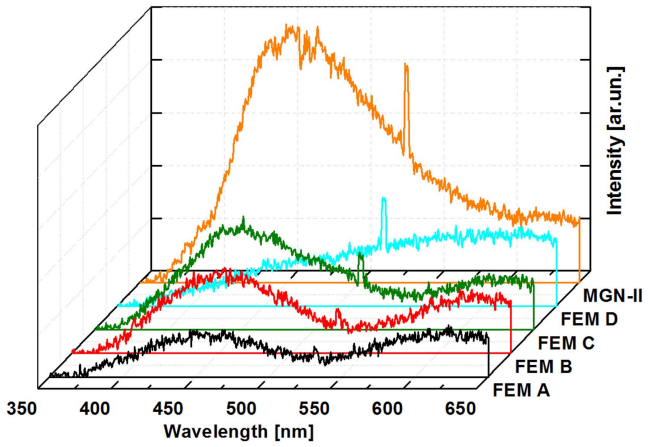


**Figure 4.** Spectrally resolved nonlinear optical responses of the laser reshaped (*MGN I*: FEM A, B, C and D) and mechanically reshaped (*MGN-II*) samples of MGN for the excitation pulse energy of 50 nJ. The spectra were processed using Savitzky–Golay smoothing filter (5 point quadratic polynomial order) for clarity in the presented data.

electron transition from 5*d*- to 6*ps*-bands [29]. It is known that in low dimensional systems the light emission is considerably enhanced by the local fields associated with the surface plasmons. Furthermore, the dielectric environment can play a significant role in the efficiency of MAIL, quenching or enhancing the signal due to different energy transfer processes.

Two maxima peaked at around 450 and 625 nm can be identified in MAIL spectra of the laser-reshaped FEM A, B and C samples, figure 4. The intensity of the blue band at ~450 nm increases with increase in Ag nano-ellipsoid aspect ratio from 2.3 to 2.6 for these samples. It is also the most intense band observed in mechanically reshaped MGN (*MGN-II*, figure 4) with the highest aspect ratio of 4.9. One may assume that the coupling into SPR improves with increasing aspect ratio of the NPs. Note that this band is suppressed in FEM D sample. This observation may be attributed to the fact that FEM D contains reshaped NPs with aspect ratios of both 2.6 and 4.1 due to the subsequent irradiation, hence quenching the signal at ~450 nm. Some background contribution into the blue band component of MAIL at 450 nm may also be attributed to $Ag^+$ ions inhomogenously distributed within the volume of the glass during the fabrication step and as a result of the $Ag^+$–$Na^+$ ion exchange process [30], and to $Ag^+$–$Ag^+$ interaction pairs due to the high concentration of the $Ag^+$ ions in the glass [31, 32].

One also observes that the MAIL spectrum of the laser-reshaped sample FEM D with an aspect ratio of 4.1 is dominated by 625 nm band, figure 4. The 625 nm MAIL band can be attributed to the small charged clusters such as $Ag_2^+$, $Ag_2^{2+}$, $Ag_3^+$ and $Ag_3^{2+}$ formed during laser-assisted reshaping. This band was also observed in the single-photon luminescence studies on laser-induced ionisation and photo-modification of Ag NPs in soda lime glass [30]. The laser-assisted reshaping, described in detail elsewhere [5], results in formation of the cationic shell in the vicinity of the Ag NPs. The density of this cationic shell is higher around the Ag nano-

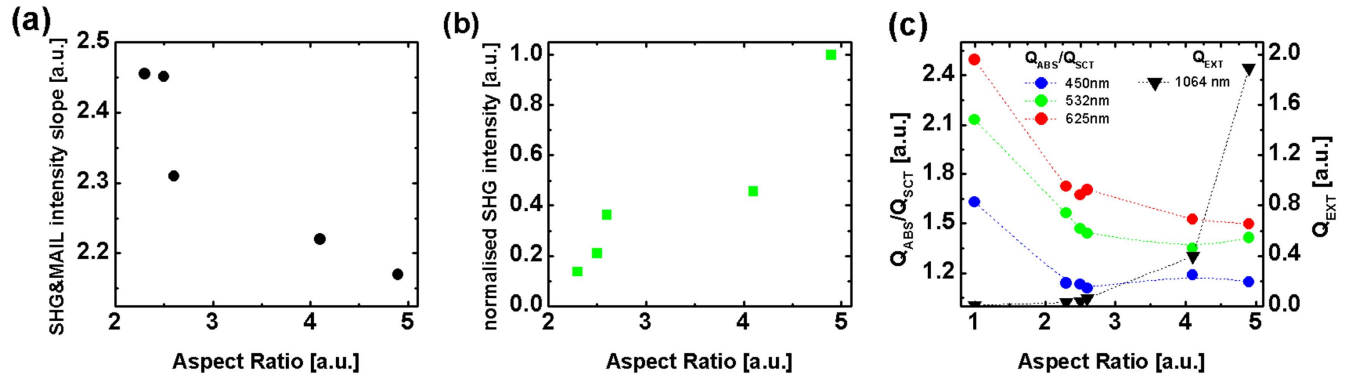


**Figure 5.** (a) SHG and MAIL integrated intensity slopes obtained for the pulse energies from 10 to 80 nJ in the MGN with corresponding aspect ratios. (b) Integrated SH signal achieved at pump pulse energy of 50 nJ in MGNs with different elongation ratios. (c) Absorption ($Q_{ABS}$), scattering ($Q_{SCT}$) at the wavelengths of 450, 532 and 625 nm and extinction ($Q_{EXT}$) at 1064 nm efficiency factors calculated using DDA.

ellipsoids with large aspect ratios. This explains the 625 nm band intensity increase observed with increase in the aspect ratio of laser-reshaped MGNs and the fact that the band is not pronounced in the MAIL spectrum of the mechanically stretched *MGN-II*.

Indeed MAIL-in contrast to SHG-involves absorption of an excitation photon followed by its re-emission in a radiative transition. As shown in [24], the difference in observed nonlinear responses from Ag nano-ellipsoids with different aspect ratios can be associated with the relative strength of scattering and absorption in NPs. It has also been shown [24] that for elongated metal NPs, there is a competition between SHG and MAIL. Figure 5(a) shows the SHG and MAIL intensity slopes achieved in our MGN samples for the excitation pulse energies between 10 and 80 nJ. For the MGN sample containing least modified NPs (*MGN I*: FEM A with aspect ratio of 2.3) the intensity slope is ~2.45, whereas for FEM D, with the estimated aspect ratio of 4.1, it falls to ~2.2, and finally to ~2.17 for the mechanically stretched (*MGN-II*) sample with aspect ratio of 4.9. Since SHG and two-photon-induced luminescence scale quadratically with intensity of the incident light, observed slope deviations may suggest that three-photon-induced processes are also present in the MAIL signal around 360 nm. Therefore, in MGNs containing Ag NPs with large aspect ratios, SHG is likely to be the dominant process (figure 5(b)).

Figure 5(c) shows the absorption ($Q_{ABS}$), scattering ($Q_{SCT}$) and extinction ($Q_{EXT}$) efficiency factors of Ag NPs with different elongation ratios estimated using the DDA method [12, 33, 34]. The Ag dielectric constant was adopted from [20]. The host medium refractive index of 1.53 was assumed to be constant in the wavelength range under consideration. The effective radius ($a_{eff}$) used for the NPs in the simulations was taken to be 15 nm. The number of dipoles, equal to a target size of 60 × 60 × 60, was kept constant and only the aspect ratio was varied in accordance with the values summarised in table 1. The incident radiation in the model was assumed to be linearly polarised along the long axis of the target reflecting the experimental conditions used. The DDA simulation results confirm that the extinction for Ag NPs at 450, 532 and 625 nm is dominated by absorption for all aspect ratios under consideration. The decrease in absorption to scattering ratio ($Q_{ABS}/Q_{SCT}$) observed for large aspect ratios (i.e. the laser-reshaped *MGN I*: FEM D and mechanically-reshaped *MGN-II* with 4.1 and 4.9 aspect ratios, respectively) also correlate with experimentally observed increase in SHG intensity (figure 5(b)).

The simulation results confirm that MAIL phenomenon is dominant in the Ag nano-ellipsoids with small aspect ratios (i.e. the laser-reshaped *MGN-I*: FEM A, B and C with estimated aspect ratios of 2.3, 2.5 and 2.6 respectively). It is worth noting that the spectrally resolved optical response in the laser-reshaped MGNs, registered in transmission geometry and shown in figure 4, can be substantially modified due to the self-absorption in reshaped and unmodified spherical Ag NPs within the NPs containing layer, as simulation results suggest for the Ag NPs with aspect ratio of 1, in figure 5(c).

## 4. Conclusions

It has been shown that both SHG and MAIL are present for ellipsoidal Ag NPs embedded in soda-lime glass. SHG and MAIL spectra were explained for *two* different types of nanoparticle reshaping mechanisms: laser reshaped (*local modification*) and mechanically stretched (*global modification*). It was argued that ion species in the vicinity of the laser reshaped NPs and small Ag ions in the volume of the NP containing layer are responsible for the observed MAIL signal in the visible range. It was concluded that competition between SHG and MAIL arises from the difference in scattering and absorption cross-sections of the NPs. It was shown that SHG is prominent for NPs with higher aspect ratios.

Both mechanical stretching and laser-assisted reshaping of the Ag NPs provide a simple and yet effective tool for spectral manipulation of the SPRs. By subsequent irradiation of MGNs with precisely chosen wavelengths, elongation effects greater than the values presented here can be achieved, leading to higher scattering cross sections and effectively

better frequency doubling abilities. Laser reshaping (unlike mechanical stretching) provides spectral selectivity, and more importantly the much needed *spatial selectivity,* for fast and local nanoprocessing of MGNs, paving the way for the fabrication of micro-patterned optical elements [35] in photonics, security and data storage [36].

## Acknowledgments

This research was conducted under the aegis of the Engineering and Physical Sciences Research Council (EPSRC) of the United Kingdom (EP/I004173/1). MAT was a Marie Curie Early Career Fellow within the LA$^3$NET Network (Grant Agreement Number 289191) at the University of Dundee when part of this work was conducted. All data created during this research are openly available from the University of Dundee Institutional Repository.

## References

[1] Kreibig U and Vollmer M 1995 *Optical Properties of Metal Clusters* (*Springer Series in Materials Science*) (Berlin: Springer)
[2] Fleming L A H, Tang G, Zolotovskaya S A and Abdolvand A 2014 Controlled modification of optical and structural properties of glass with embedded silver nanoparticles by nanosecond pulsed laser irradiation *Opt. Mater. Express* **4** (5) 969
[3] Tyrk M A, Gillespie W A, Seifert G and Abdolvand A 2013 Picosecond pulsed laser induced shape transformation of metallic nanoparticles embedded in a glass matrix *Opt. Express* **21** 21823–8
[4] Stalmashonak A, Graener G and Seifert G 2009 Transformation of silver nanospheres embedded in glass to nanodisks using circularly polarized femtosecond pulses *Appl. Phys. Lett.* **94** 193111
[5] Stalmashonak A, Seifert G and Abdolvand A 2013 *Ultra-short Pulsed Laser Engineered Metal-Glass Nanocomposite* (*SpringerBrief in Physics*) (Berlin: Springer)
[6] Kaempfe M, Rainer T, Berg K-J, Seifert G and Graener H 1999 Ultrashort laser pulse induced deformation of silver nanoparticles in glass *Appl. Phys. Lett.* **74** 1200
[7] Doster J, Baraldi G, Gonzalo J, Solis J, Hernandez-Rueda J and Siegel J 2014 Tailoring the surface plasmon resonance of embedded silver nanoparticles by combining nano- and femtosecond laser pulses *Appl. Phys. Lett.* **104** 153106
[8] Baraldi G, Gonzalo J, Solis J and Siegel J 2013 Reorganizing and shaping of embedded near-coalescence silver nanoparticles with off-resonance femtosecond laser pulses *Nanotechnology* **24** 255301
[9] Tyrk M A, Zolotovskaya S A, Gillespie W A and Abdolvand A 2015 Radially and azimuthally polarized laser induced shape transformation of embedded metallic nanoparticles in glass *Opt. Express* **23** 23394–400
[10] https://codixx.de/en/home.html
[11] Podlipensky A, Lange J, Seifert G, Graener H and Cravetchi I 2003 Second-harmonic generation from ellipsoidal silver nanoparticles embedded in silica glass *Opt. Lett.* **28** 716–8
[12] Draine B T 1988 The discrete-dipole approximation and its application to interstellar graphite grains *Astrophys. J.* **333** 848–72
[13] Quaranta A, Cattaruzza E and Gonella F 2008 Modelling the ion exchange process in glass: phenomenological approaches and perspectives *Mater. Sci. Eng.* B **149** 133–9
[14] Opilski A, Rogozinski R, Gut K, Blahut M and Opilski Z 2000 Present state and perspective involving application of ion exchange in glass *Opto-Electron. Rev.* **8** 117–27
[15] Berg K-J, Berger A and Hofmeister H 1991 Small silver particle in glass-surface layers produced by sodium-silver ion-exchange-their concentration and size depth profile *Z. Phys.* D **20** 309–11
[16] Gans R 1915 Über die form ultramikroskopischer silberteilchen *Ann. Phys.* **47** 270–84
[17] Papavassiliou G C 1979 Properties of small inorganic and organic metal particles *Prog. Solid State Chem.* **12** 185–271
[18] Link S, Mohamed M B and El-Sayed M A 1999 Simulation of the optical absorption spectra of gold nanorods as a function of their aspect ratio and the effect of the medium dielectric constant *J. Phys. Chem.* B **103** 3073–7
[19] Link S and El-Sayed M A 1999 Simulation of the optical absorption spectra of gold nanorods as a function of their aspect ratio and the effect of the medium dielectric constant *J. Phys. Chem.* B **103** 3073–7
Link S and El-Sayed M A 2005 *J. Phys. Chem.* B **109** 10531–2 erratum
[20] Johnson P B and Christy R W 1972 Optical constants of the noble metals *Phys. Rev.* B **6** 4370–9
[21] Hofmeister H, Drost W-G and Berger A 1999 Orientated prolate silver nanoparticles in glass-characteristics of novel dichroic polarizers *Nanostr. Mat.* **12** 207–10
[22] Stalmashonak A, Unal A A, Graener H and Seifert G 2009 Effects of temperature on laser-induced shape modification of silver nanoparticles embedded in glass *J. Phys. Chem.* C **113** 12028–32
[23] Eichelbaum M, Schmidt B E, Ibrahim H and Rademann K 2007 Three-photon-induced luminescence of gold nanoparticles embedded in and located on the surface of glassy nanolayers *Nanotechnology* **18** 355702
[24] Deng H-D, Li G-C, Dai Q-F, Ouyang M, Lan S, Trofimov V A and Lysak T M 2013 Size dependent competition between second harmonic generation and two-photon luminescence observed in gold nanoparticles *Nanotechnology* **24** 075201
[25] Boyd G T, Yu Z H and Shen Y R 1986 Photoinduced luminescence from the noble metals and its enhancement on roughened surfaces *Phys. Rev.* B **33** 7923–36
[26] Farrer R A, Butterfield F L, Chen V W and Fourkas J T 2005 Highly efficient multiphoton-absorption-induced luminescence from gold nanoparticles *Nano Lett.* **5** 1139–42
[27] Dowling M B, Li L, Park J, Kumi G, Nan A, Ghandehari H, Fourkas J T and DeShong P 2010 Multiphoton-absorption-induced-luminescence (MAIL) Imaging of tumor-targeted gold nanoparticles *Bioconjugate Chem.* **21** 1968–77
[28] Dai D C, Xu S J, Shi S I and Xie M H 2005 Efficient multiphoton-absorption-induced luminescence in single-crystalline ZnO at room temperature *Opt. Lett.* **30** 3377–9
[29] Mooradian A 1969 Photoluminescence of metals *Phys. Rev. Lett.* **22** 185
[30] Podlipensky A V, Grebenev V, Seifert G and Graener H 2004 Ionization and photomodification of Ag nanoparticles in soda-lime glass by 150 fs laser irradiation: a luminescence study *J. Lumin.* **109** 135–42
[31] Cattaruzza E, Mardegan M, Trave E, Battaglin G, Calvelli P, Enrichi F and Gonella F 2011 Modifications in silver-doped silicate glasses induced by ns laser beams *Appl. Surf. Sci.* **257** 5434–8
[32] Borsella E, Battaglin G, García M A, Gonella F, Mazzoldi P, Polloni R and Quaranta A 2000 Structural incorporation of silver in soda-lime glass by the ion-exchange process: a

photoluminescence spectroscopy study *Appl. Phys.* A **71** 125–32

[33] Draine B T and Goodman J 1993 Beyond clausius-mossotti: wave propagation on a polarizable point lattice and the discrete dipole approximation *Astrophys. J.* **405** 685–97

[34] Draine B T and Flatau P J 1994 Discrete dipole approximation for scattering calculations *J. Opt. Soc. Am.* A **11** 1491–9

[35] Seifert G, Unal A A, Skrzypczak U, Podlipensky A, Abdolvand A and Graener H 2009 Toward the production of micropolarizers by irradiation of composite glasses with silver nanoparticles *Appl. Opt.* **48** F38–44

[36] Stalmashonak Andrei, Abdolvand Amin and Seifert Gerhard 2011 Metal-glass nanocomposite for optical storage of information *Appl. Phys. Lett.* **99** (20) 201904